Chapter 3

Synthesis & Characterization of,

SiW_{12} anchored to Hβ (SiW_{12}/Hβ)

as well as

SiW_{11} anchored to zeolite Hβ (SiW_{11}/Hβ)

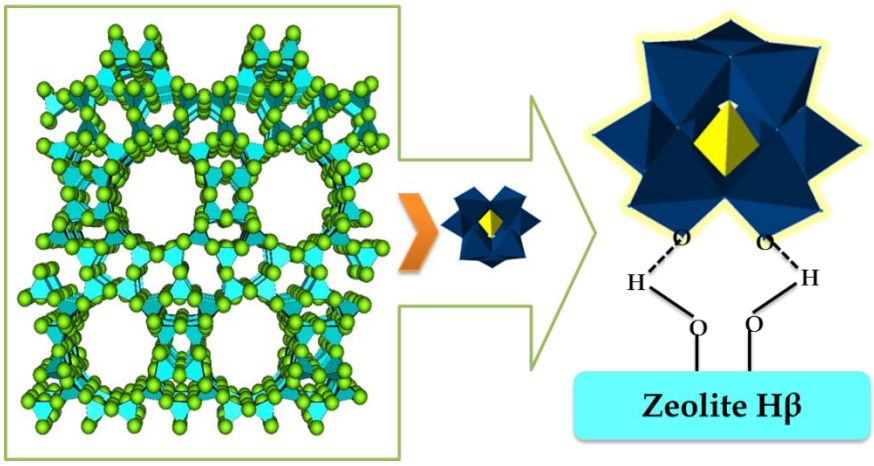

Zeolites are crystalline aluminosilicates whose structure is formed by an array of corner-sharing SiO_4^{4-} or AlO_4^{5-} tetrahedra [1-2]. These building blocks become arranged in a periodic way to form channels and cages on a nano- and sub nano-meter scale of strictly regular dimensions, named micropores. The pores of the zeolites are open to the exterior and to the surrounding medium, thus allowing diffusion of molecules from the exterior to the interior of the zeolite particle. The existence of these accessible micropores ranks zeolites at the top of the list of solids exhibiting large specific surface areas, typically above 300 m^2/g with an internal void volume above 0.1 cm^3/g [3].

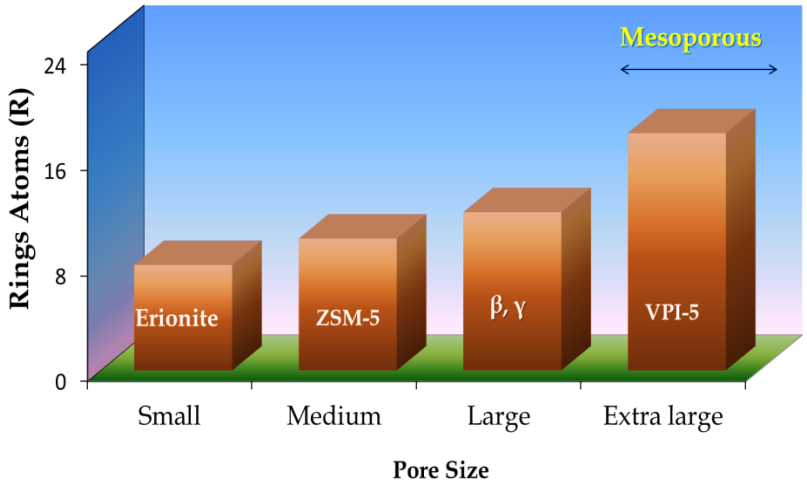

Chart 1. Classification of zeolites on the basis of pore dimensions.

Zeolites are classified based on the symmetry of their unit cell, each structure being denoted by three capital letters. [4] An alternative classification that is more convenient here is according to the dimensions of the micropores (Chart 1). In this regard the zeolites can be classified as having a small, medium or large pore size depending on whether the number of oxygen atoms and Si plus Al atoms is 8, 10 or 12, respectively [5]. There has been an intense search for large-pore zeolites (those having pores with 12-membered rings), the aspect of importance regarding the micropore system of zeolites is the geometry of the pores. In this regard, zeolites can be classified as one, two and three

directional zeolites, depending on whether the channel system is arranged along one, two or the three Cartesian axes. The directionality of the zeolite pore system is relevant with respect to the ability of zeolites to include guests inside the micropores.

Zeolites are easy to separate from the reaction products, thereby offering convenient reactor design and allowing continuous-flow operation. Because they are thermally stable and chemically robust, zeolites can be completely regenerated by calcination in air when they become deactivated by the presence of large organic products that remain adsorbed. The promising results of zeolites in acid-base catalysis have triggered an intense research effort aimed at development of functional and encapsulated materials. In this context there are few articles reporting the synthesis of catalysts containing zeolites and POMs having properties of both.

Lee et al. [6] in 1986, for the first time used Y-zeolite as a support for encapsulation of $H_3PW_{12}O_{40}$, $H_4SiW_{12}O_{40}$, $H_4SiMo_{12}O_{40}$ and $H_3PMo_{12}O_{40}$. They demonstrated alkylation of toluene with methanol in a fixed bed reactor with a continuous flow system. Catalysts impregnated with lower amount of POMs showed higher initial activity, and the catalytic activity was enhanced by more electronegative metal ion of POMs salt impregnated on Y-zeolite. Catalyst impregnated with $BiPMo_{12}O_{40}$ showed a good activity and a good regeneration ability of catalytic activity.

Richter et al. [7] synthesized a medium-pore zeolite ZSM-5 modified by impregnation with an aqueous solution of $H_4SiW_{12}O_{40}$. Ethylbenzene conversion and m-xylene isomerization was used as the catalytic probe reactions. They showed that the Keggin unit cannot penetrate the ZSM-5 pore system but merely becomes deposited on the external zeolite surface. It was believed that the specific modification of external molecular-sieve surfaces by a

metallic (hydrogenating) component could be extended to other elements as well, provided that there exist a polyanion with a molecular size larger than the mean pore size of the molecular sieve to be modified. Sulikowski and group synthesized $H_3PW_{12}O_{40}$ anchored to dealuminated zeolite Y, containing a secondary pore system with the predominant pore radii of 15 Å [8]. The interaction between the PW_{12} and the zeolite matrix has been studied using ^{29}Si, ^{27}Al and ^{31}P MAS NMR. Increased acidic properties of the PW_{12}/zeolite Y system were demonstrated by a change in the selectivity pattern of *m*-xylene transformations in the gas phase.

Mukai and group [9] in 2001 studied the influence of properties of zeolite support on the amount of encapsulation of Keggin-type, $H_3PMo_{12}O_{40}$ in the supercages of Y-type zeolite. By controlling number of aluminum atoms in the zeolite framework, they succeeded in enhancing the catalytic activity of the encapsulated catalyst. Later in 2003, they made an effort to improve the preparation method of "ship-in-the-bottle" type $H_3PMo_{12}O_{40}$ anchored Y-type zeolite [10]. They studied the influence of temperature and solvent addition during synthesis on the amount of $H_3PMo_{12}O_{40}$ loading and the stability of the resulting catalyst were investigated.

Anandan and Yoon [11] made an unconventional attempt to prepare $H_3PW_{12}O_{40}$ encapsulated TiHY zeolite as a new photocatalyst mimicking the plant photosynthetic system. This photocatalyst was observed to generate hydrogen and oxygen from the aqueous solutions upon illumination by two photon reactions (UV and visible lights), which was quite analogous to the "Z-scheme" mechanism for plant photosynthetic systems. The turnover number of the photocatalyst was determined to be 11 with the quantum yield of the water splitting about 27 ± 6% at 352 nm.

Ren et al. [12] demonstrated esterification of acetic acid with n-butanol in the liquid-phase over $H_3PW_{12}O_{40}$ and its cesium salts anchored to dealuminated ultra-stable Y zeolite. The anchored $Cs_{2.5}H_{0.5}PW_{12}O_{40}$ catalyst gave a high conversion of n-butanol of 94.6% and selectivity for n-butyl acetate of 100%, accompanying the high water-tolerance and catalytic reusability without regeneration.

Wang and group $H_3PW_{12}O_{40}$ and its cesium salt anchored on dealuminated ultra-stable zeolite Y (DUSY) with various loadings were prepared by impregnation method, and their catalytic performances were evaluated in the liquid-phase acetalization of ethyl acetoacetate with ethylene glycol to fructone. High catalytic activity was found over the anchored catalysts [13].

Jun et al. [14], in order to solve the serious leaching problem of anchored POMs in polar reaction media, $H_3PMo_{12}O_{40}$ encapsulated in the supercage of Cs^+-exchanged zeolite Y was prepared by the "ship in the bottle" synthesis. The influence of ion-exchange conditions as well as the synthesis parameters on the encapsulation of $H_3PMo_{12}O_{40}$ were investigated and were found to influence the process remarkably. Catalytic study on esterification of acetic acid with n-butanol was also carried out. Under the optimal conditions, $H_3PMo_{12}O_{40}$ could be successfully encapsulated in the supercage of CsY zeolite, and the samples showed considerable catalytic activity and excellent reusability in the esterification reaction.

Zendehdel et al. prepared and characterized a series of hybrid $H_3PW_{12}O_{40}$ (HPA/NaY and HPA/NaY/MCM-41) [15]. BET and XRD showed blocking of the pore particles by HPA. The catalytic activity was carried out for preparation of 2-(4-nitrophenyl)- 2,3-dihydro-1*H*-perimidine. Results exhibited higher yields with use of HPA/NaY and HPA/NaY/MCM-41. The formation

of perimidine was affected by the pores diameter and the Bronsted acidity of the catalysts.

Atalay and Gunduz [16] reported liquid phase isomerization of α-pinene over $H_3PW_{12}O_{40}$ anchored to natural zeolite rich in clinoptiolite in a batch slurry reactor in a nitrogen atmosphere and at constant temperature of 373 K. The catalytic activity increased from 15% to 99% with the introduction of POM at 4.25 wt% onto the natural zeolite. However, the catalytic activity decreased with the calcination of the catalyst. The isomerization reaction of α-pinene resulted into camphene and limonene with selectivities of about 40% and 3%, respectively, over the POM anchored on natural zeolite.

Pizzio and group [17] reported two series of materials based on $H_3PW_{12}O_{40}$ immobilized on NH_4Y and NH_4ZSM-5 zeolites by wet impregnation method. The catalysts were characterized by various physicochemical techniques and it was observed that for NH_4YTPA_{05} catalyst, $[PW_{12}O_{40}]^{3-}$ anion was partially transformed into $[P_2W_{21}O_{71}]^{6-}$ anion during the synthesis and drying steps. The photocatalytic activity for 4-chlorophenol degradation was also carried out. They can be reused at least three times without decrease in the degradation degrees.

Zeolite beta is a high silica zeolite with large pores. It is highly disordered, made up of an intergrowth of two or more polymorphs comprising a three-dimensional system of 12-membered ring channels [18] having pore diameters of 0.76 × 0.64 nm and 0.55 × 0.55 nm. Owing to large pore size, surface area, and pore volume with controllable Si/Al ratios accompanied by ion-exchange capacity, zeolite beta is a good candidate for catalysis. It possesses high thermal and chemical stability, surface silanol groups and hydrophobic character which are the characteristics of ideal support [18].

Literature survey shows that there is no work reported on silicotungstates anchored to zeolite Hβ. In the present work, we describe synthesis and physicochemical as well as spectroscopic characterization of two series of catalysts, silicotungstic acid (SiW_{12}) as well as monolacunary silicotungstate (SiW_{11}) anchored to zeolite Hβ. The support and the catalysts were characterized by elemental analysis (EDS), thermo gravimetric analysis (TGA), Fourier Transform Infrared Spectroscopy (FT-IR), Laser-Raman Spectroscopy, X-ray diffraction (XRD), surface area measurement (BET method), pore size, pore volume and ^{29}Si MAS-NMR (Magic-Angle Spinning- Nuclear Magnetic Resonance) studies. Further, the surface morphology of support and catalysts was studied by Scanning Electron Microscopy (SEM) and Transmission Electron Microscopy (TEM). The strength as well as type of acidic sites was determined by n-butylamine potentiometric titrations.

EXPERIMENTAL

Materials

All the chemicals used were of A.R. grade. Sodium tungstate, sodium silicate, n-butylamine, 12-tungstosilicic acid and acetone were purchased from Merck. Sodium form of Zeolite Beta (β) with Si/Al ratio 10 was procured from Zeolites and Allied Products, Bombay, India, and used as received.

Treatment of the support (Naβ to Hβ)

The zeolite support (Naβ) was converted in to NH_4^+ form by conventional ion exchange method using a 10 wt. %, 1M NH_4Cl aqueous solution [19]. The resulted NH_4^+ type zeolite was further converted to H^+ type by calcination in air at 550 ^oC for 6 h.

Synthesis of mono lacunary silicotungstate, $Na_8SiW_{11}O_{39}.11\ H_2O$ (SiW_{11})

SiW_{11} was synthesized by following the same method described in Chapter 1. 0.22 mol, 7.2 g sodium tungstate and 0.02 mol, 0.56 g sodium silicate were dissolved in 150 mL distilled water at 80 ^oC. The pH was then adjusted to 4.8 by dilute nitric acid. The volume of the mixture was reduced to half and the resulting solution was filtered to remove unreacted silicates. The lacunary polyoxometalate anion was separated by liquid-liquid extraction with acetone. The extraction was repeated until the acetone extract showed the absence of nitrate ions. The extracted sodium salt of mono lacunary silicotungstate was dried at room temperature in air. The resulting material was designated as SiW_{11}.

Synthesis of the catalysts

SiW_{12} anchored to Hβ

SiW_{12} was anchored to Hβ by impregnation method. 1g of Hβ was impregnated with an aqueous solution of SiW_{12} (0.1g/10 mL of distilled water). The water from the suspension was allowed to evaporate at 100 °C in an oven. Then the resulting mixture was dried at 100 °C with stirring for 10h. The material thus obtained was designated as 10% SiW_{12}/Hβ. Same procedure was followed for the synthesis of a series of SiW_{12} anchored catalyst (0.2-0.4 g/20-40 mL of distilled water). The obtained materials were designated as 20% SiW_{12}/Hβ, 30% SiW_{12}/Hβ and 40% SiW_{12}/Hβ, respectively.

SiW_{11} anchored to Hβ

SiW_{11} was anchored to Hβ by impregnation method. 1g of Hβ was impregnated with an aqueous solution of SiW_{11} (0.1g/10 mL of distilled water). The water from the suspension was allowed to evaporate at 100 °C in an oven. Then the mixture was dried at 100 °C with stirring for 10h. The obtained material was treated with 0.1 N HCl, filtered, washed with distilled water and dried at 100 °C. Same procedure was followed for the synthesis of a series of SiW_{11} anchored catalyst (0.2-0.4 g/20-40 mL of distilled water). The obtained materials were designated as 20% SiW_{11}/Hβ, 30% SiW_{11}/Hβ and 40% SiW_{11}/Hβ, respectively.

RESULTS AND DISCUSSION

Characterization of SiW_{12} as well as SiW_{11} anchored to Hβ

Leaching Test

Any leaching of the catalyst from the support would make the catalyst unattractive. So, it is necessary to study the stability of polyanion onto support in order to reuse the catalyst. When the polyoxometalate react with a mild reducing agent such as ascorbic acid [20], it develops blue coloration, which can be used for the quantitative characterization for the leaching of polyoxometalate from the support. In the current work, we have used this method for determining the leaching of SiW_{12}/SiW_{11} from Hβ support.

Standard samples amounting to 1-5% of SiW_{12}/SiW_{11} in water were prepared. To 10 mL of the above samples, 1 mL of 10% ascorbic acid was added. The mixture was diluted to 25 mL. The resultant solution was scanned at a λ_{max} of 785 nm for its absorbance values. A standard calibration curve was obtained by plotting values of absorbance with percentage solution. One gram of 30% SiW_{12}/Hβ as well as 30% SiW_{11}/Hβ was refluxed for 4h with 10 mL of conductivity water. 1 mL of the supernant solution was then treated with 10% ascorbic acid. No development of blue color indicates no leaching. The same procedure was repeated with water, methanol, glycerol and also with the filtrates of all the reaction mixtures after completion of the reaction. The above procedure was followed for all catalysts and no leaching was found. For each case, absence of blue color indicates no leaching of SiW_{12}/SiW_{11} from support into reaction medium. The study indicates the presence of chemical interaction between the SiW_{12}/SiW_{11} and Hβ, as well as stability of the resultant catalysts under reaction conditions.

BET Surface Area

Table 1. Textural properties of support and catalysts.

Catalyst	Surface area (m^2/g)	Pore diameter d(nm)	Pore volume (cm^3/g)
Hβ	587.2	2.48	0.267
10% SiW_{12}/Hβ	448.3	1.79	0.189
20% SiW_{12}/Hβ	428.5	1.71	0.175
30% SiW_{12}/Hβ	419.2	1.68	0.157
40% SiW_{12}/Hβ	315.1	0.75	0.102
10% SiW_{11}/Hβ	458.2	1.85	0.195
20% SiW_{11}/Hβ	449.1	1.78	0.180
30% SiW_{11}/Hβ	439.8	1.71	0.169
40% SiW_{11}/Hβ	320.4	0.70	0.113

Table 1 shows specific surface area and pore diameter of both the catalysts and support. The specific surface area and pore diameter of Hβ was found to be decreased after inclusion of SiW_{12}/SiW_{11}. The incorporation of SiW_{12} into the framework of the support is apparent here, as it leads to ~28% reduction in surface area as well as ~32% reduction in pore width for 30% SiW_{12}/Hβ. This indicates that SiW_{12} occupies sites inside the zeolite framework. The decrease in pore diameter of the catalyst is due to the presence of SiW_{12} inside the zeolite framework, as anticipated. Similar trend was observed in the case of 30% SiW_{11}/Hβ. However, both surface area and pore diameter of 30% SiW_{11}/Hβ are higher than those of 30% SiW_{12}/Hβ. This may be due to the fact that the removal of W-O unit from the parent SiW_{12} results in decrease in the

size of SiW_{11} species leading to the increase in the available space inside the channels of the support.

As the % loading increases surface area, pore diameter and pore volume all strongly decreases. This confirms that the active species are located quite inside the framework of the support. Further, up to 30% loading constant decrease in the surface area was observed which may be due to the monolayer formation of the active species. Further increase in loading up to 40% leads to the drastic decrease in the surface area as well as pore diameter due to blocking of the framework channels. As a result 30% loaded catalysts were selected for the further characterizations.

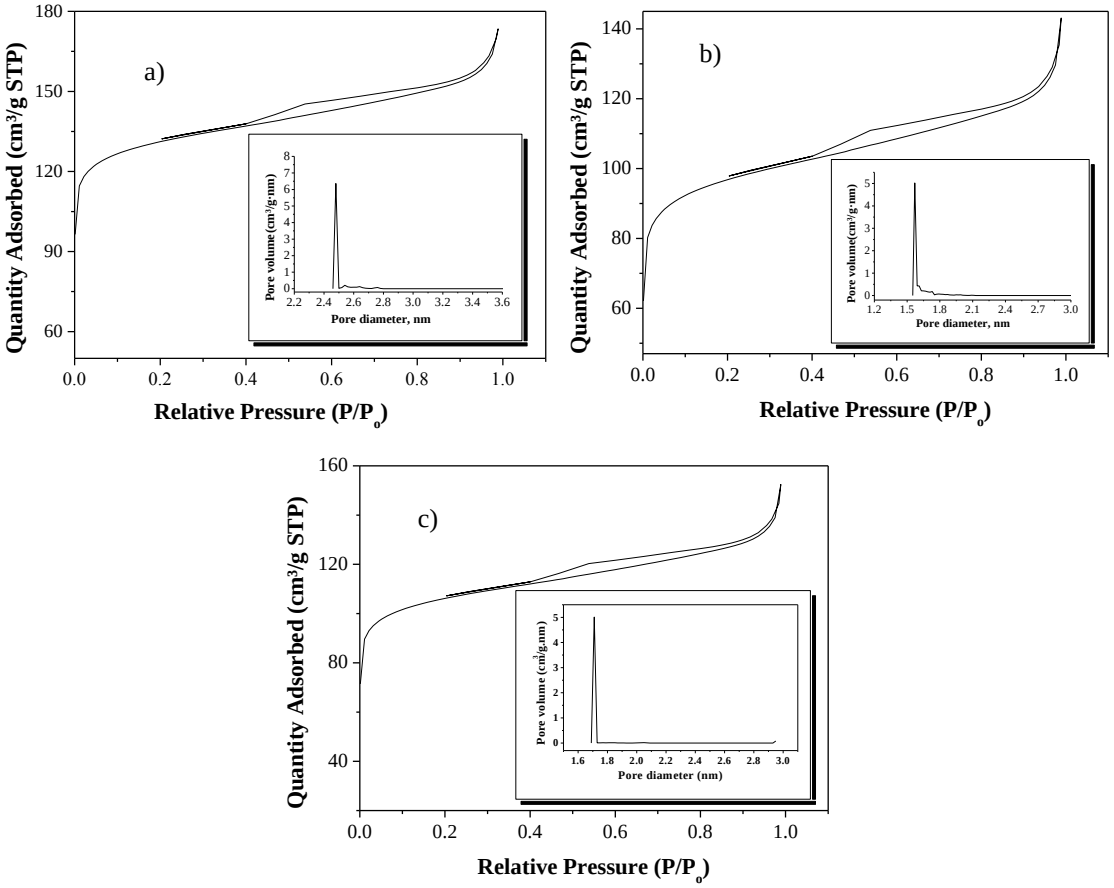

Figure 1. Nitrogen sorption isotherms and pore size distributions (inset) of a) Hβ, b) 30% SiW_{12}/Hβ and c) 30% SiW_{11}/Hβ.

The N_2 adsorption–desorption isotherms as well as pore size distributions of Hβ, 30% SiW_{12}/Hβ and 30% SiW_{11}/Hβ are shown in Figure 1. All the N_2 adsorption–desorption isotherms showed *type I* pattern with three stages: monolayer adsorption of nitrogen on the walls of pores at P/Po < 0.4, the part characterized by a sharp increase in adsorption due to capillary condensation in mesopores with hysteresis at P/P_o = 0.4 - 0.8, and multilayer adsorption on the outer surface. The pore size distributions in the inset show that all the samples have narrow pore size distribution within the micropore range. The overall decrease in surface area of both the catalysts with respect to the support gives the first indication of a chemical interaction between SiW_{11}/SiW_{12} and Hβ.

Elemental Analysis

Table 2. EDS elemental analysis.

Materials	Elemental analysis (weight %)					
	Theoretical			EDS		
	Al	Si	W	Al	Si	W
30% SiW_{12}/Hβ	2.5	26	17.6	2.2	26.6	18.5
30% SiW_{11}/Hβ	2.9	26.9	16.7	2.2	27.6	16.5

The EDS elemental analysis for 30% SiW_{12}/Hβ and 30% SiW_{11}/Hβ is shown in Table 2. The results obtained from EDS were in good agreement with the analytically calculated values.

Thermal Analysis

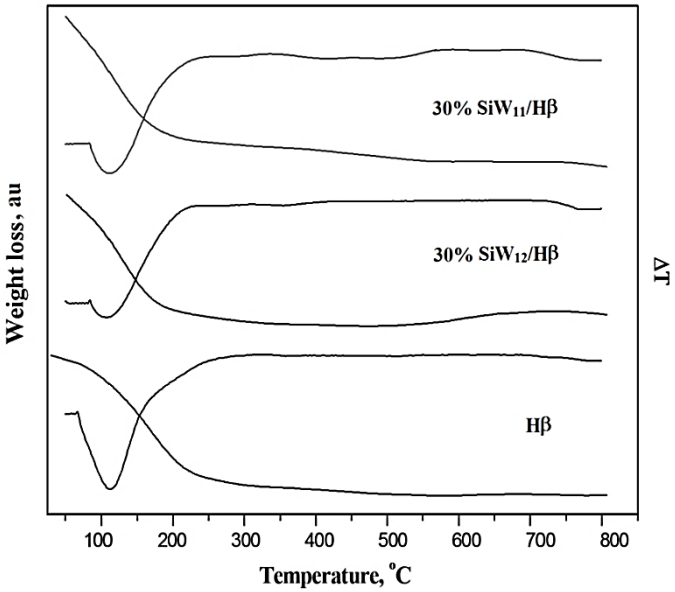

Figure 2. TG-DTA of Hβ, 30% SiW_{12}/Hβ and 30% SiW_{11}/Hβ.

TGA-DTA curves of Hβ, 30% SiW_{12}/Hβ and 30% SiW_{11}/ Hβ are displayed in Figure 2. A unique weight loss of 13-15 % was observed up to 250 ^{o}C for Hβ, which is attributed to desorption of physically adsorbed water. No further weight loss was observed beyond 250 ^{o}C which indicates zeolite Hβ retains its framework structure up to 600 ^{o}C. For the catalyst 30% SiW_{12}/Hβ, similar weight loss of 10-12 % up to 200 ^{o}C assigned to adsorbed water was detected. Second gradual weight loss of 1.2-1.5 % was observed between 200-300 ^{o}C due to the loss of water of crystallization of Keggin anion. TGA analysis suggests that 30% SiW_{12}/Hβ is stable up to 480 ^{o}C.

The TGA of 30% SiW_{11}/Hβ (Figure 2) shows initial weight of 6% up to 170 ^{o}C may be due to the removal of adsorbed water molecules. Second weight loss of 2% has been observed up to 240 ^{o}C which is due to loss of water of crystallization. No notable loss up to 410 ^{o}C indicates the stability of the catalyst up to 410 ^{o}C.

The TGA data shows that anchoring of SiW_{12}/SiW_{11} to Hβ increases the thermal stability. An increase in thermal stability indicates the presence strong interaction between SiW_{12}/SiW_{11} and Hβ.

Fourier Transform Infrared Spectroscopy

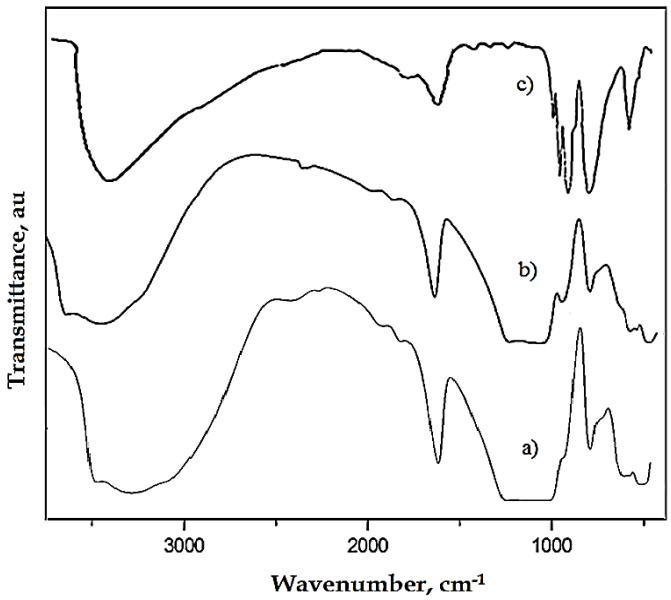

Figure 3. FT-IR spectra of a) Hβ, b) 30% SiW_{12}/Hβ and c) SiW_{12}.

FT-IR of SiW_{12} (Figure 3) has four characteristic bands at 1020, 926, 878, and 779 cm^{-1} corresponding to W=O_d asymmetrical, Si-O_a asymmetrical, W-O_b-W asymmetrical, and W-O_c-W asymmetrical respectively. Where O_a, O_b, O_c, and O_d attributed to the oxygen atoms connected to silicon, to oxygen atoms bridging to two tungsten (from two different triads for O_b and from the same triad for O_c), and to the terminal oxygen W=O, respectively. FT-IR spectra for Hβ and 30% SiW_{12}/ Hβ (Figure 3) shows large and broad peak appearing in range of 1020-1090 cm^{-1} is due to asymmetric stretching vibration O-T-O (ν_{asym}), which is sensitive to the silicon and aluminium contents in the zeolite Hβ framework. A broad band between 3700 and 3200 cm^{-1} is assigned as hydrogen bonds of silanol groups. The typical band for SiW_{12}, at 920 cm^{-1} corresponding to Si-O_a (ν_{asym}), is clearly observed in 30% SiW_{12}/Hβ. FT-IR

spectra indicate that the SiW_{12} anions preserve Keggin unit even after anchoring to the support.

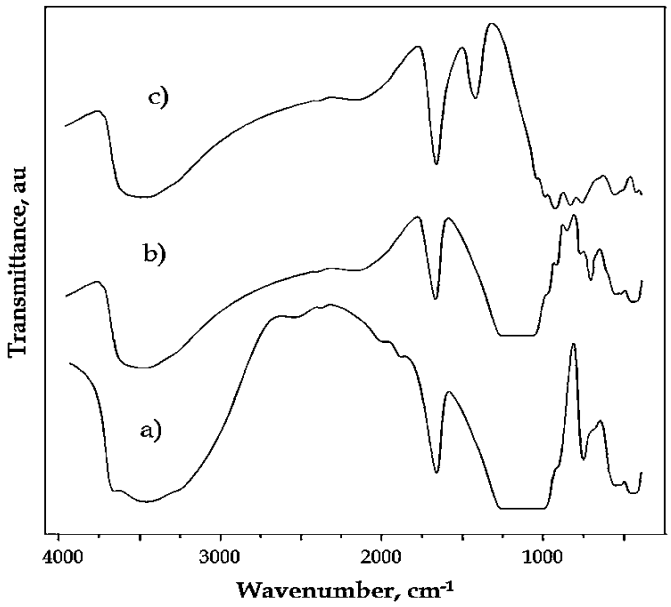

Fig. 4. FT-IR Spectra of a) Hβ, b) 30% SiW_{11}/Hβ and c) SiW_{11}.

The FT-IR spectrum of SiW_{11} (Figure 4) shows bands at 98 cm^{-1} (W=O_d), 948 cm^{-1} (Si-O_a), 886 and 795 cm^{-1} (W- O_b -W) and 727 cm^{-1} (W- O_c -W). Where O_a, O_b, O_c, and O_d attributed to the oxygen atoms connected to silicon, to oxygen atoms bridging to two tungsten (from two different triads for O_b and from the same triad for O_c), and to the terminal oxygen W=O, respectively. This is in good agreement with the reported one [21]. FT-IR spectra for Hβ and 30% SiW_{11}/Hβ (Figure 4) shows large and broad peak appearing in range of 1000-1300 cm^{-1} is due to asymmetric stretching vibration O-T-O (ν_{asym}), which is sensitive to the silicon and aluminium contents in the zeolite Hβ framework. A broad band between 3700 and 3200 cm^{-1} is assigned as hydrogen bonds of silanol groups. The typical band for SiW_{11}, at 942 cm^{-1} (Si-O_a), 860 cm^{-1} (W- O_b -W) and 715 cm^{-1} (W- O_c -W) are clearly observed for 30% SiW_{11}/Hβ. FT-IR spectra indicate that the SiW_{11} preserves its Keggin ion unit even after

anchoring to the support. The significant shift in the bands indicates the strong chemical interaction between SiW_{11} and Hβ.

FT-Raman Spectroscopy

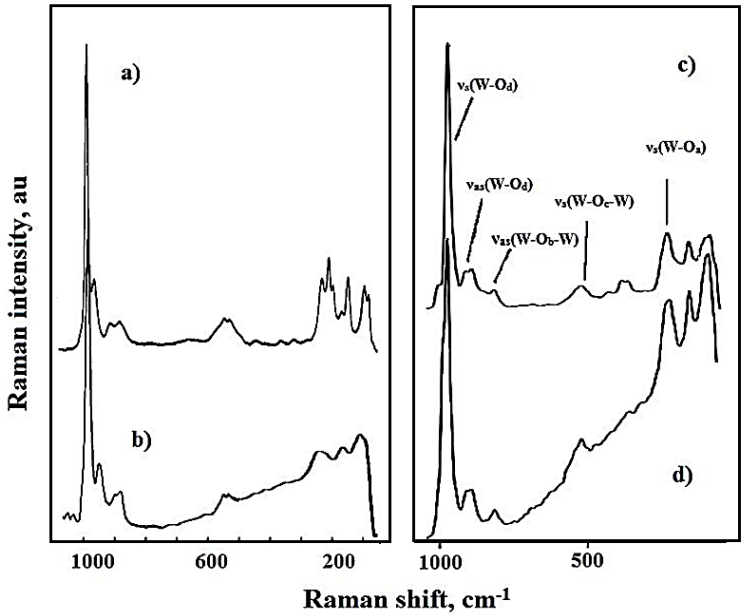

Figure 5. FT-Raman Spectra of a) SiW_{12}, b) 30% SiW_{12}/Hβ, c) SiW_{11} and d) 30% SiW_{11}/Hβ.

FT-Raman of SiW_{12} shows bands at 1054, 976, 888, 565 and 208 which are attributed to $\nu_s(W{=}O_d)$, $\nu_{as}(W{=}O_d)$, $\nu_{as}(W\text{-}O_b\text{-}W)$, $\nu_s(W\text{-}O_c\text{-}W)$, and $\nu_s(W\text{-}O_a)$, respectively (Figure 5). The Raman spectrum of 30% SiW_{12}/Hβ shows the retention of all the typical bands of SiW_{12} at 1020, 973, 911, 521 and 231 due to $\nu_s(W{=}O_d)$, $\nu_{as}(W{=}O_d)$, $\nu_{as}(W\text{-}O_b\text{-}W)$, $\nu_s(W\text{-}O_c\text{-}W)$, and $\nu_s(W\text{-}O_a)$, respectively. FT-Raman of SiW_{11} shows bands at 970, 890, 814, 521 and 231 which are attributed to $\nu_s(W\text{-}O_d)$, $\nu_{as}(W\text{-}O_d)$, $\nu_{as}(W\text{-}O_b\text{-}W)$, $\nu_s(W\text{-}O_c\text{-}W)$, and ν_s $(W\text{-}O_a)$, respectively. The FT-Raman spectrum of 30% SiW_{11}/Hβ shows the retention of 973 (ν_s $(W\text{-}O_d)$), 891 (ν_{as} $(W\text{-}O_d)$), 813 ($\nu_s(W\text{-}O_b\text{-}W)$), 519 ($\nu_s(W\text{-}O_c\text{-}W)$) and 223 ($\nu_s$ $(W\text{-}O_a)$,) bands which indicates that the structure of SiW_{11} has been retained after anchoring to the support. Remarkable shifts in the Raman bands for the

catalysts confirm the strong interaction of SiW_{12}/SiW_{11} with the hydrogen of silanol group (Si-OH) inside the channels of the support.

^{29}Si MAS- NMR Studies

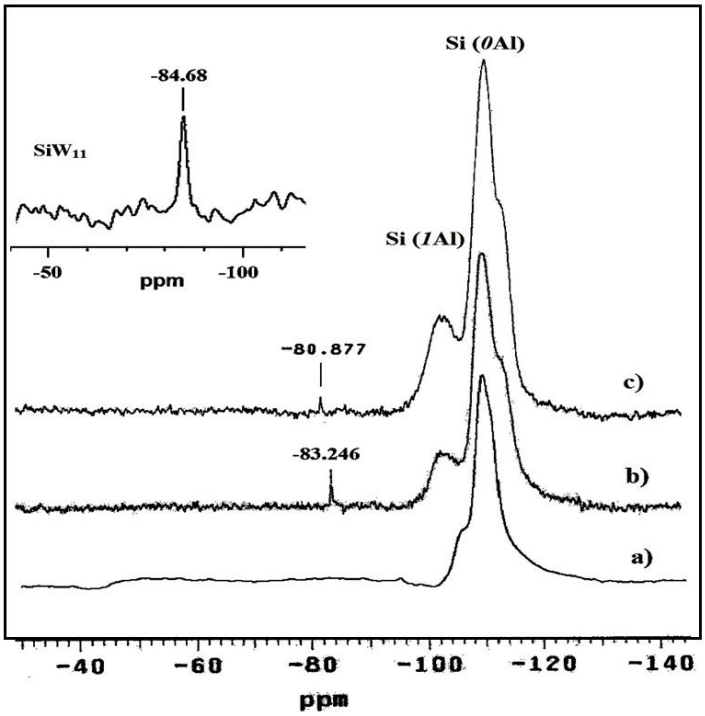

Figure 6. ^{29}Si-MAS NMR spectra of a) Hβ, b) 30% SiW_{12}/Hβ and c) 30% SiW_{11}/Hβ.

Figure 6 shows ^{29}Si-MAS NMR spectrum of Hβ, 30% SiW_{12}/Hβ and 30% SiW_{11}/Hβ. Typical characteristic peaks for SiW_{12} (-83.2) and SiW_{11} (-80.8) were observed for 30% SiW_{12}/Hβ and 30% SiW_{11}/Hβ, respectively. This confirms that SiW_{12}/SiW_{11} remains intact even after anchoring to the support. Further, two different types of silicon nuclei Si(*O*Al) (at-109.6 for 30% SiW_{12}/Hβ and -109.4 for 30% SiW_{11}/Hβ) and Si(*1*Al)) (at-101.9 for 30% SiW_{12}/Hβ and -101.8 for 30% SiW_{11}/Hβ) were observed. These two peaks are identical to those observed for support, Si(*O*Al) at -111.9 and Si(*1*Al) at -104.53. The shift as well as broadening of these peaks in the catalysts confirms the strong interaction between terminal oxygens of SiW_{12}/SiW_{11} and silanol groups of the support.

The BET, FT-IR, FT-Raman and ^{29}Si MAS-NMR analyses confirm the presence of strong hydrogen bonding between intact SiW_{12}/SiW_{11} and H of the Si-OH group of the zeolite framework. To study the dispersion of active species inside the zeolite framework, the catalysts were further characterized by XRD, SEM, and TEM analysis.

X-ray Diffraction

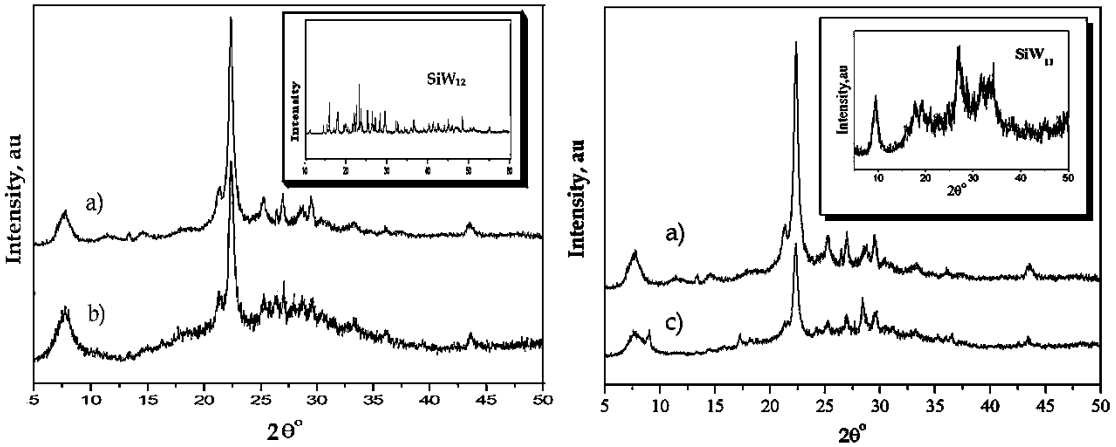

Figure 7. X-ray diffraction patterns of a) Hβ, b) 30% SiW_{12}/Hβ and c) 30% SiW_{11}/Hβ.

XRD of the catalysts show crystalline peaks with respect to zeolite framework (Figure 7) suggesting that structure of Hβ has been retained after incorporation of SiW_{12}/SiW_{11}. The intensity of the reflections in the catalysts was lower as compared to the support. The catalysts show reflections of POMs with very low intensity indicating a well dispersion of SiW_{12}/SiW_{11} inside the channels of the support [22, 23]. The homogeneous dispersion of SiW_{12}/SiW_{11} was further confirmed by SEM and TEM analyses.

Scanning Electron Microscopy

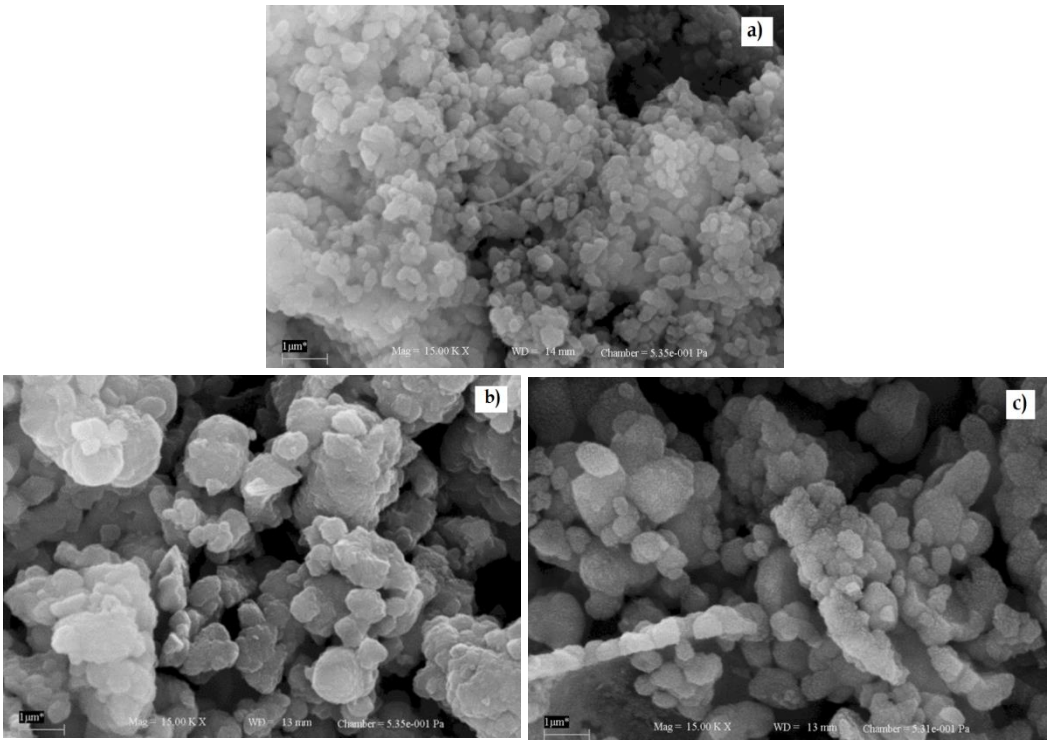

Figure 8. SEM images of a) Hβ, b) 30% SiW_{12}/Hβ and c) 30% SiW_{11}/Hβ.

The SEM images show that the surface morphology of the catalysts (Figure 8b and 8c) is identical to that of Hβ (Figure 8a). The absence of aggregates of SiW_{12}/SiW_{11} species in the catalyst suggests that POMs species are well dispersed inside the zeolite channels [23]. The results are in good agreement with the XRD analysis.

Transmission Electron Microscopy

The TEM image of Hβ (Figure 9a) at 50 nm resolution displays the porous surface morphology with uniform pore sizes. The TEM images of the catalysts (Figure 9b and 9c) shows uniform porous morphology over very large scales very identical to the support. The absence of crystallites of SiW_{12}/SiW_{11} indicates that the active species are well dispersed inside the micro pores of the zeolite support with retention of uniform porous structure (inset Figure 9c).

TEM analysis confirms the retention of identical zeolite framework as well as uniform dispersion of the active species.

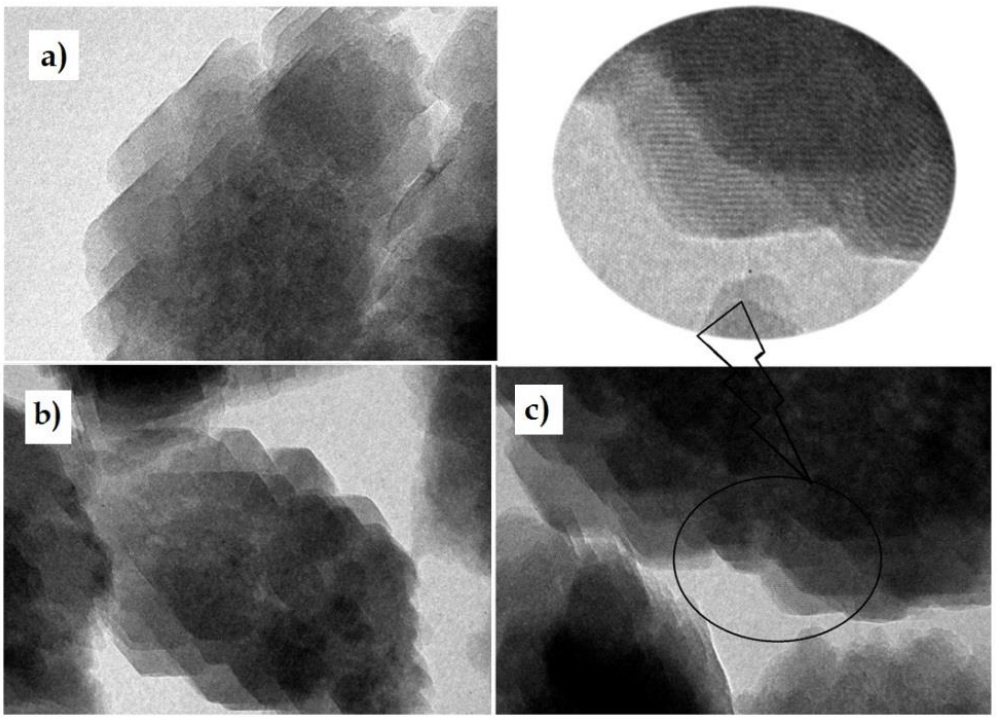

Figure 9. TEM images of a) Hβ, b) 30% SiW_{12}/Hβ and c) 30% SiW_{11}/Hβ.

Acidity Measurements

The plot of the potential as a function of meq of n-butylamine/g of the catalysts and support is shown in Figure 10. It was observed that, the support and catalysts contain very strong acid sites. The strength of acidic sites in terms of initial electrode potential is shown in Table 3. It is clear from the Table 3 that the incorporation of species SiW_{12}/SiW_{11} increases the strength of the acid sites of catalysts to a great extent.

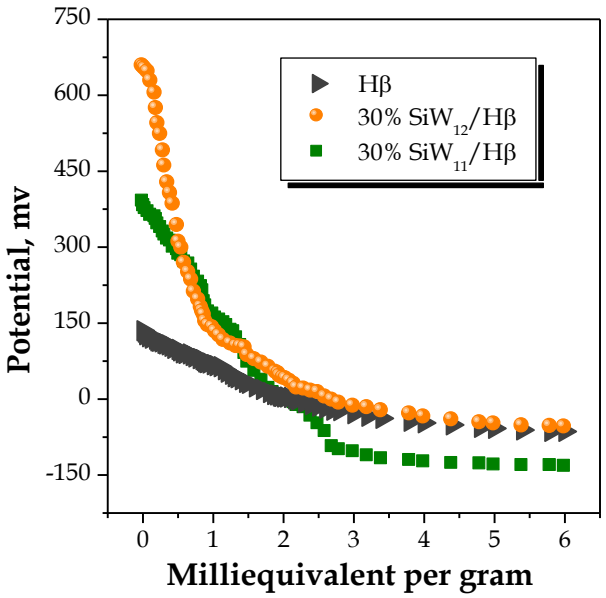

Figure 10. Potentiometric titration curves of support and catalysts.

It is also interesting to note that there is a drastic decrease in the acidic strength of 30% SiW_{11}/Hβ as compared to 30% SiW_{12}/Hβ. The reason being, the acidic character of POMs is mainly due to the acidic addenda atoms i.e. tungsten in the present case and removal of one tungsten-oxygen unit from the parent SiW_{12} is expected to decrease the acidity of the SiW_{11}. The obtained value is in good agreement with the expected one.

Table 3. Potentiometric n-butylamine acidity of support and the catalysts.

Material	Acidic strength, mV	Types of acid sites[a]	
		very strong	strong
Hβ	135	0.44	2.10
30% SiW_{12}/Hβ	657	1.46	2.60
30% SiW_{11}/Hβ	390	1.40	2.16

[a] meq. of n-butylamine per gram of catalyst

Conclusions

- In conclusion, we have come up with *new heterogeneous catalysts* comprising of parent as well as lacunary *silicotungstates anchored to Hβ*.
- Zeolite Hβ was synthesized by converting commercially available Naβ in to *ammonium form* and subsequently to *proton* form by calcination.
- XRD, SEM and TEM confirm the *retention* of Hβ framework in the synthesized catalysts.
- Thermal stability of SiW_{12}/SiW_{11} *increases* after anchoring on to Hβ, and catalysts, 30% SiW_{12}/Hβ and 30% SiW_{11}/Hβ were *stable* up to 410-480 ^{o}C.
- FT-IR and Raman spectra show that *Keggin ion structure* of SiW_{12}/SiW_{11} *remains intact* even after anchoring on to Hβ.
- BET surface area, ^{29}Si MAS-NMR data and Raman studies show that there is a *strong interaction*, hydrogen bonding, between surface oxygens of SiW_{12}/SiW_{11} with Hβ. From spectroscopic characterization, the interaction between the support and SiW_{12}/SiW_{11} is as follows,

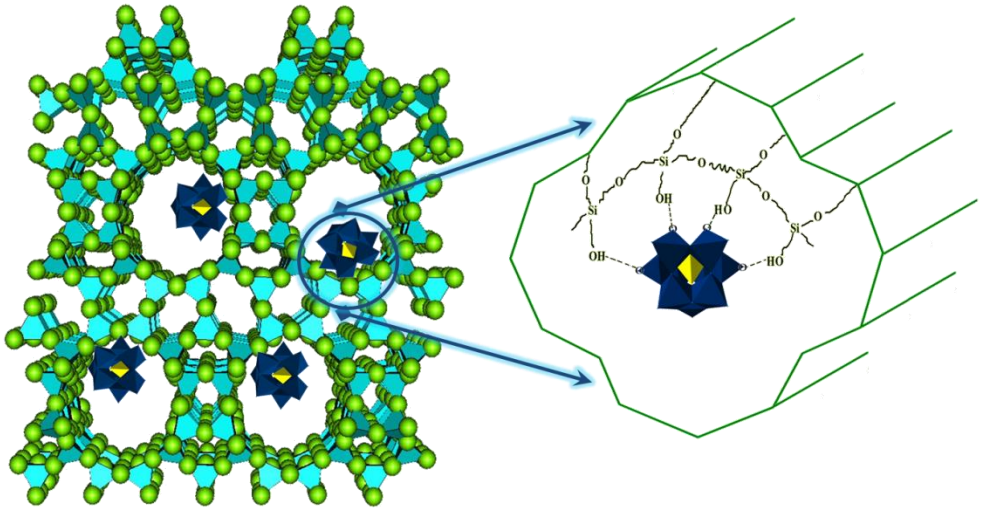

- XRD, SEM, and TEM studies reveal that both SiW_{12} and SiW_{11} are *uniformly dispersed* inside the channels *without disturbing* the framework structure of Hβ.

References

1. R. M. Barrer, *Zeolites and Clay Minerals as Sorbents and Molecular Sieves*, Academic Press, London, (1978).
2. D. W. Breck, *Zeolite Molecular Sieves: Structure, Chemistry and Use*, John Wiley and Sons, New York, (1974).
3. A. Corma, H. Garcia, Eur. J. Inorg. Chem., 1143, (2004).
4. W. M. Meier, D. H. Olson, C. Baerlocher, Zeolites, 17, (1), (1996).
5. M. E. Davis, Acc. Chem. Res., 26, 111, (1993).
6. C. Y. Hwang, J. W. Kwak, W. Y. Lee and H. L. Lee, Korean J. of Chem. Eng., 3(1), 31 (1986).
7. M. Richter, J. Janchen, H.-G. Jerschkewitz, B. Parlitz and E. Schreier, J. Chem. Soc. Faraday Trans., 87(9), 1461, (1991).
8. Z. Olejniczak, B. Sulikowski, A. Kubacka and M. Gasior, Top. Catal., 11, 391, (2000).
9. S. R. Mukai, L. Lin, T. Masuda, K. Hashimoto, Chem. Eng. Sci., 56, 799, (2001).
10. S. R. Mukai, M. Shimoda, L. Lin, H. Tamona, T. Masuda, Appl.Catal. A: Gen., 256, 107, (2003).
11. S. Anandan, M. Yoon, J. Photochem. Photobiology A: Chem. 160, 181, (2003).
12. F. -M. Zhang, J. Wang, C. -S. Yuan, X. -Q. Ren, Catal. Lett., 102, 3, (2005).
13. F. Zhang, C. Yuan, J. Wang, Y. Kong, H. Zhu, C. Wang, J. Mol. Catal. A: Chem., 247, 130, (2006).
14. W. Ruiping, G. Maiping, W. Jun, Chin. J. Chem. Eng., 17, 58, (2009).
15. M. Zendehdel, A. Mobinikhaledi, H. Alikhani and N. Jafari, J. Chin. Chem. Soc., 57, 683, (2010).
16. B. Atalay, G. Gunduz, Chem. Eng. J. 168, 1311, (2011).
17. C. L. Marchena, R. A. Frenzel, S. Gomez, L. B. Pierella, L. R. Pizzio, Appl. Catal. B: Env., 130, 187, (2013).

18. R. M. Barrer, *Hydrothermal Chemistry of Zeolites.* London: Academic Press (1982).
19. A. Patel, N. Narkhede, Energy Fuels, 26, 6025 (2012).
20. G. D. Yadav, V. V. Bokade, Appl. Catal. A: Gen., 147, 299, (1996).
21. Y. Yang, Y. Guo, C. Hu and E. Wang, Appl. Catal. A: Gen., 252, 305, (2003).
22. R. Wei, M. Guo and J. Wang, Chin. J. Chem. Eng., 17, 58, (2009).
23. O. da Silva Lacerda Jr., R. Marinho Cavalcanti, T. Moreira de Matos, R. S. Angélica, G. N. da Rocha Filho, I. de Carvalho Lopes Barros, Fuel, 108, 604, (2013).